ISSN 0016-7037
Volume 73, Number 4
February 15, 2009

Geochimica et Cosmochimica Acta

JOURNAL OF THE GEOCHEMICAL SOCIETY
AND THE METEORITICAL SOCIETY

Volume 73, Number 4 February 15, 2009

Articles

Continued on outside back cover

Available online at www.sciencedirect.com
ScienceDirect
Geochimica et Cosmochimica Acta 73 (2009) 1039–1051
Geochimica et Cosmochimica Acta
www.elsevier.com/locate/gca

Diffusion of ^{40}Ar in muscovite

T. Mark Harrison [a,b,*], Julien Célérier [b], Amos B. Aikman [b], Joerg Hermann [b], Matthew T. Heizler [c]

[a] Institute of Geophysics and PlanetaryPhysics and Department of Earth and Space Sciences, University of California, Los Angeles, CA 90095, USA
[b] Research School of Earth Sciences, The Australian National University, Canberra, ACT 0200, Australia
[c] New Mexico Bureau of Geology and Mineral Resources, New Mexico Tech, 801 Leroy Place, Socorro, NM 87801, USA

Received 24 April 2008; accepted in revised form 9 September 2008; available online 6 December 2008

Abstract

Hydrothermal treatment of closely sized muscovite aggregates in a piston-cylinder apparatus induced $^{40}Ar^{*}$ loss that is revealed in $^{40}Ar/^{39}Ar$ step heating spectra. Age spectra and Arrhenius data, however, differ from that expected from a single diffusion length scale. A numerical model of episodic loss assuming the presence of multiple diffusion domains yields excellent fits between synthetic and actual degassing spectra. We used this model to isolate $^{40}Ar^{*}$ loss from the grains that remained intact during hydrothermal treatment at 10 kbar permitting calculation of diffusion coefficients in the temperature range 730-600 °C. Diffusion data generated in this manner yield an activation energy (E) of 63 ± 7 kcal/mol and frequency factor (D_o) of $2.3\ ^{+70}_{-2.2}$ cm^2/s. Experiments at 20 kbar yield diffusivities lower by about an order of magnitude and correspond to an activation volume of ~14 cm^3/mol. Together, these parameters predict substantially greater retentivity of Ar in muscovite than previously assumed and correspond to a closure temperature (T_c) of 425 °C for a 100 μm radius grain cooling at 10 °C/Ma at 10 kbar ($T_c = 405$ °C at 5 kbar. Age and log (r/r_o) spectra for the run products show strong correlations indicating that muscovites can retain Ar diffusion boundaries and mechanisms that define their natural retentivity during vacuum step heating. This may permit the application of high resolution, continuous $^{40}Ar/^{39}Ar$ thermochronology to low grade, regionally metamorphosed terranes.

1. INTRODUCTION

Muscovite is one of the most utilized minerals in $^{40}Ar/^{39}Ar$ thermochronology due to its high potassium content, low tendency to incorporate excess radiogenic ^{40}Ar ($^{40}Ar^{*}$), and ubiquitous presence in low grade, regionally metamorphosed terranes (McDougall and Harrison, 1999). Given its widespread use in thermochronology, it is thus surprising that no published study of Ar diffusion in muscovite – a requirement for calculating closure temperature (T_c) – has yet appeared. Instead, the thermochronological community has tended to adopt a nominal T_c value of ca. 350 °C (e.g., Hodges, 1991), based in part on historical calibrations of age vs. metamorphic grade (e.g., Purdy and Jäger, 1976).

The relationship between the diffusion coefficient (D) and the absolute temperature (T) is given by the Arrhenius equation:

$$D = D_o \exp(-E/RT) \quad (1)$$

where E is activation energy, D_o the frequency factor, and R is the gas constant (kcal/mol-K). If $^{40}Ar^{*}$ transport occurs via volume diffusion, diffusion coefficients should array on an Arrhenius plot (i.e., log D vs. $1/T$). Arrhenius parameters, E and D_o, for Ar diffusion have been experimentally-

* Corresponding author. Address: Institute of Geophysics and Planetary Physics and Department of Earth and Space Sciences, University of California, Los Angeles, CA 90095, USA. Fax: +1 310 825 7970.
E-mail address: tmark.harrison@gmail.com (T.M. Harrison).

0016-7037/$ - see front matter © 2008 Elsevier Ltd. All rights reserved.
doi:10.1016/j.gca.2008.09.038

derived for several hydrous silicates used in $^{40}Ar/^{39}Ar$ thermochronology: phlogopite (Giletti, 1974), hornblende (Harrison, 1981; Baldwin et al., 1990), and biotite (Harrison et al., 1985; Grove and Harrison, 1996). These studies utilized the bulk-loss method involving hydrothermal treatment of uniformly sized, mono-mineralic aggregates. The run products were then analyzed by the K–Ar or $^{40}Ar/^{39}Ar$ methods and the resultant $^{40}Ar^*$ loss calculated by comparing treated and untreated samples.

The only experimental Ar diffusion study of muscovite is an M.S. Thesis in which 18 hydrothermal experiments on sized micas were undertaken (Robbins, 1972). Diffusion coefficients were calculated from bulk-loss data obtained from isotope dilution measurements of $^{40}Ar^*$ concentrations. The results yielded a linear Arrhenius relationship with an E of 40 kcal/mol and a D_o of 6.3×10^{-7} cm^2/s assuming a plane sheet diffusion geometry. An equivalent case was made for the infinite cylinder geometry with a similar E but a D_o 500 times higher (due to the width to thickness ratio of mica grains). Hames and Bowring (1994) reinterpreted these data in light of natural $^{40}Ar^*$ gradients observed in muscovites that appeared inconsistent with diffusion occurring perpendicular to the c-axis. They calculated an E of 43 ± 9 kcal/mol and a D_o of 4×10^{-4} cm^2/s for an infinite cylinder model. Lister and Baldwin (1996) subsequently argued that the Robbins (1972) data were best fit via a plane sheet geometry with a characteristic plate thickness of ~12 μm. Both studies noted the relatively unretentive behavior of Ar in muscovite predicted by Robbins (1972) results.

The lack of a follow up to Robbins (1972) study probably reflects limitations imposed by the relatively small temperature range over which such experiments can be made. Experimental runs need to be conducted at sufficiently high temperatures for measurable Ar diffusion to occur, but not so high as to exceed the stability field of muscovite (Chatterjee and Johannes, 1974; Evans, 1965). A lower bound of ~600 °C is dictated by the small degree of Ar equilibration expected below this temperature (i.e., <5% $^{40}Ar^*$ loss is predicted for a 20 μm grain after 3 months heating at 600 °C). Ultrahigh lateral resolution *in situ* methods such as SIMS or RBS could in principle access lower temperatures but do not have adequate sensitivity to measure ppm quantities of Ar (Ryerson, 1987). Laser Ar microprobes have revealed ^{40}Ar gradients in annealed feldspars over 10's of μm length scales, but do not have the spatial resolution or sensitivity to be useful in this kind of study (see McDougall and Harrison, 1999). At the other end of the possible temperature range, dehydration breakdown of muscovite in the presence of water occurs in the 600–700 °C temperature range between 1 and 3 kbar (Evans, 1965). Because Robbins (1972) used an experimental apparatus capable of a maximum pressure of ~2 kbar, his study was thus limited to ⩽700 °C. This relatively restricted field in log D vs. $1/T$ space provides little leverage with which to precisely constrain E.

Undertaking experiments in a piston-cylinder apparatus enables runs at much higher pressure and thus over a greater range of temperatures than a cold-seal vessel. Although higher temperature increases diffusivity, the corresponding pressure increase slows diffusion requiring the trade off between increasing pressure and temperature along the univariant reaction curve to be assessed. Assuming the Arrhenius parameters and activation volume for biotite (Grove and Harrison, 1996; Harrison et al., 1985) as an analogue suggests that overall increases in diffusivity will occur with increasing pressure and temperature along the muscovite stability boundary.

The sensitivity of mass spectrometers used today is up to 100 times greater than the K–Ar method used by Robbins (1972) and the $^{40}Ar/^{39}Ar$ approach permits 10× better precision (i.e., ±0.1% vs. ±1%; McDougall and Harrison, 1999). Thus small ^{40}Ar losses from very small samples can now be meaningfully measured (e.g., Grove and Harrison, 1996).

In this study, we revisited Ar diffusion in muscovite by taking advantage of the methodological advances described above. Our higher resolution data reveal more complicated diffusion behavior than previously assumed, but permit refined estimates of Ar retentivity under laboratory conditions which in turn leads to improved estimates of T_c.

2. MUSCOVITE SAMPLE

To obtain meaningful Ar diffusion parameters in a bulk-loss type experiment, it is imperative that the phase of interest remain stable throughout the heating experiment, or at least that any instability be restricted to a small volume fraction relative to the degree of Ar loss. We assessed the characteristics of two candidate starting materials in this role: muscovites ANU 82-315 and MUS-1. Run products from four hydrothermal experiments between 700 and 800 °C at 10 kbar using the ~3 Ga muscovite ANU 82-315 (Wijbrans, 1985) all showed complete breakdown of muscovite (Célérier, 2007). Electron imaging of the untreated sample showed it to contain opaque inclusions and occasional quartz grains. Despite careful handpicking, sufficient contaminants remained in the mineral separate that substantially reduced the stability field of muscovite. We then examined the behavior of muscovite MUS-1, a 15 × 10 cm book from a pegmatite, Harts Range, Central Australia. The mica was sized by repeated hand-grinding and sieving to produce sized fractions with average radii of 24 ± 4, 56 ± 6, and 87 ± 10 μm as calculated using the approach of Grove and Harrison (1996). Despite thorough sieving, however, we observed that the sized populations typically contains ~5% of grains much smaller than the nominal size (Fig. 1), apparently due to electrostatic adherence to larger grains. Ultrasonic treatment of the separates following hand-grinding did not remove the smaller grains.

To establish whether $^{40}Ar^*$ is uniformly distributed throughout the MUS-1 starting material, an aliquot of the 38–53 μm size fraction was analyzed by the $^{40}Ar/^{39}Ar$ step heating method (Electronic annex EA-1). The age spectrum (Fig. 2) is uniform over >90% of gas release from which we infer that the sample has been essentially closed to loss of ^{40}Ar since 325.8 ± 2.5 Ma. A representative chemical analysis of the starting material is given in Table 1.

3. EXPERIMENTAL METHODS

Sized fractions of the MUS-1 starting material were loaded and sealed (using a carbon arc welder) into 2.3 or

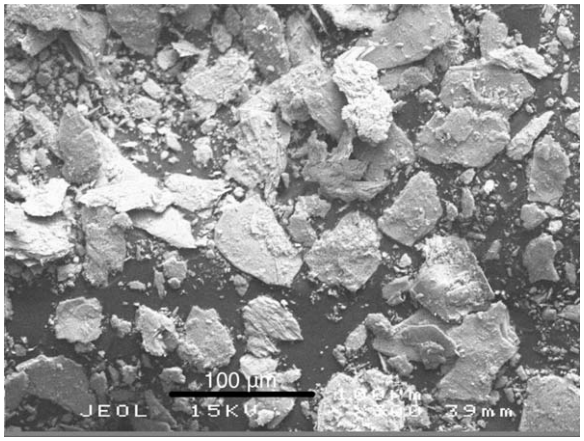

Fig. 1. Backscattered electron image of the untreated, sized (38–53 µm), starting material (MUS-1) used in the diffusion study.

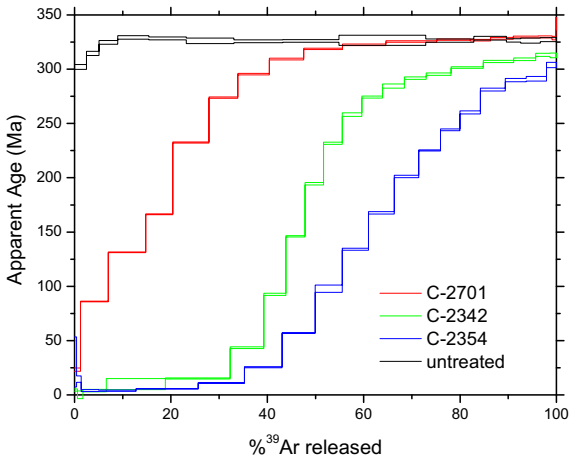

Fig. 2. $^{40}Ar/^{39}Ar$ age spectra of the untreated starting material MUS-1 (black) together with representative examples of hydrothermally treated muscovites (see Electronic annexes EA-1 and EA-2).

Table 1
Representative EMPA analysis of starting material.

Oxide	Weight %
SiO_2	45.35
TiO_2	0.75
Al_2O_3	31.53
FeO[a]	4.06
MnO	<0.1
MgO	1.21
CaO	<0.1
Na_2O	0.66
K_2O	10.6
Total	94.16

[a] Total iron as FeO.

3.5 mm diameter Au capsules along with $Al(OH)_3$ (5:1 sample to buffer) to buffer Al_2O_3 and H_2O activities. Two experiments (D-786, D-787) run in Pt capsules of the same size and starting material/buffer proportions as the Au capsules experienced hydrogen loss resulting in muscovite instability (results not reported here). Including $Al(OH)_3$ has the advantage of achieving hydrothermal conditions ($P_{H_2O} = P_{total}$) without the necessity of introducing free water which might tend to dissolve mica. A single experiment (C-2675) was run without the addition of $Al(OH)_3$ in order to investigate the behavior of the muscovite under 'dry' experimental conditions.

A Pt-Rh thermocouple at the top of the capsules monitored sample temperature with an accuracy of ±10 °C. Experiments were run in the piston-cylinder apparatus at 10 kbar (±1 kbar for experiments <2 days, ±0.5 kbar for experiments >2 days) and temperatures of 600, 630, 660, 680, and 730 °C ensuring that run conditions were well within the stability field of muscovite. Three runs were performed at 20 kbar (680 and 730 °C) to assess the role of pressure on diffusivity. Run durations varied from 10 min to 55 days. On completion of each run, samples were quenched (~10 s) and recovered from the capsules.

Following removal from their capsules, run products were handpicked to remove most of the entrained Au fragments and Al_2O_3. Run products were examined by SEM to assess muscovite stability, the chemical composition relative to the untreated sample, and whether dissolution or grain growth occurred during treatment.

Neutron irradiations were undertaken in several batches and analyzed by the $^{40}Ar/^{39}Ar$ step heating method to determine $^{40}Ar^*$ loss. Products of the first and second irradiations (ANU 125 and ANU 137) using Cd shielding in the HIFAR reactor (Tetley et al., 1980) were analyzed with the ANU VG3600 mass spectrometer using FC-2 sanidine (28.02 Ma; Renne et al., 1998) as a flux monitor (Electronic annex EA-1). Following irradiation in the D-3 position of the Texas A&M reactor together with FC-2 sanidine, the remaining run products were analyzed using the MAP 215-50 mass spectrometer at New Mexico Tech (Electronic annex EA-2). Analytical methods are described in Heizler et al. (1999). Differences in neutron flux and hardness between the two reactors are unlikely to affect Ar diffusion behavior. All results are reported in Electronic annexes EA-1 and EA-2 using the decay constants and ^{40}K abundances recommended by Stieger and Jäger (1977).

4. BULK-LOSS RESULTS

Electron micrograph examination of run products show that the grain size distribution of all Au encapsulated hydrothermally treated samples is broadly similar to that of the untreated material (Célérier, 2007). Run products are dominated (>90%) by grains of the original size, but also contain smaller grains. Relative to the starting material, treated grains are typified by less cleanly defined crystal surfaces and grains appear to be somewhat creased and slightly bent, though remain intact. Occasional grains of corundum (crystallized from $Al(OH)_3$) were also seen in the SEM images (Fig. 3c).

Textural relationships shows that little, if any, neoformed muscovite growth occurred during the <700 °C runs, and that the populations of small grains are essen-

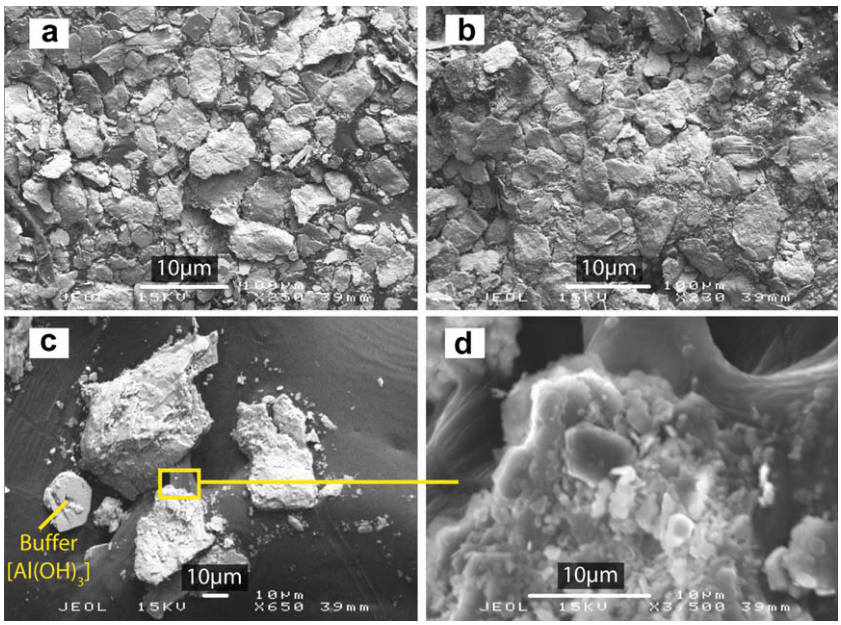

Fig. 3. Representative SEM images of hydrothermally treated muscovite. (a) Backscattered electron image of C-2342. (b) Backscattered electron image of C-2358. (c) Backscattered electron image of C-2354 highlighting the thin veneer of recrystallized grains which decorate the exterior of the muscovites run at 730 °C. Also indicated is a euhedral grain of corundum formed from buffer decomposition. (d) Close inspection of the surface of a muscovite grain from C-2354 shows minor amounts of neoformed muscovite.

tially equal in proportion to those in the starting material (Fig. 3). However, at 730 °C, small, euhedral, muscovite grains appear (Fig. 3). These grains form a thin veneer decorating the surfaces of the original muscovites, are characteristically small (typically <5 μm), and account for <5% of the total volume. In all cases, it is clear that the original texture (and grain size distribution) of the sized separate is largely preserved.

Spot chemical analyses show that treated muscovite grains have slightly higher Al and lower Si values relative to the untreated starting material (Fig. 4). Furthermore,

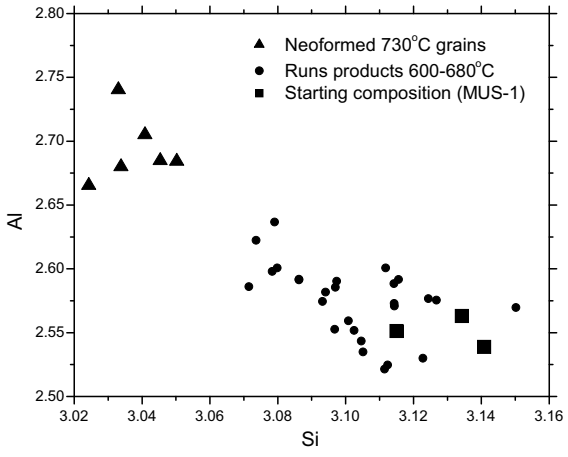

Fig. 4. Plot of Si and Al (normalized to their stoichiometric values) in MUS-1 samples. Squares show the composition of the untreated starting material, circles the non-recrystallized run products and triangles the composition of small, neoformed grains observed only in the 730 °C experiments.

the small, neoformed muscovite grains crystallized in the 730 °C runs (typified in Fig. 3c) plot in unique Al–Si space relative to the untreated muscovites (Fig. 4). They vary by <1 wt% in SiO_2 and Al_2O_3 relative to the starting material and grains treated at lower temperature account for <5% of the sample mass. The higher Al (and lower Si) contents relative to the starting material almost certainly reflects the buffering of Al_2O_3 during hydrothermal treatment.

Although we did not calculate D for C-2675 (run without the addition of $Al(OH)_3$; Table 2), we note that relative to C-2358 (run under the same conditions but with buffer), this run experienced ~10% less fractional loss. This may reflect the fact that a fluid phase is a necessary reservoir for $^{40}Ar^*$ to be diffusively lost from muscovite during the experiments.

$^{40}Ar/^{39}Ar$ age spectra (Electronic annexes EA-1 and EA-2; representative examples shown in Fig. 2) indicate that significant ^{40}Ar loss was achieved in every experiment, with essentially zero ages in the early degassing climbing gradually towards the age of the untreated material in the later steps. The significance of the shape of the age spectra are discussed later. The three runs in which hydrothermal conditions were not maintained during treatment (D-786, D-787, C-2623) are distinguished by complete degassing at lower temperatures. Clearly, muscovite was not stable through these runs and their results are not considered further.

Assuming the measured size is the diffusion length scale (see Giletti, 1974; Harrison et al., 1985; Grove and Harrison, 1996), bulk diffusivities calculated using an spherical model for the 16 experiments at 10 kbar in which muscovite remained stable (Table 2) yield an E of ~44 kcal/mol (Fig. 5). Although this is similar to what

Table 2
Results of Ar diffusion in muscovite experiments.

Run #	Temp. (°C)	Pressure (kbar)	Time (h)	Grain radius (μm)	Age (Ma)	*Fo*	*D* (cm^2/s)	log *D*
C-2342	730	10	132.0	24	167.6	0.00753	9.13E-14	−13.04
C-2354	730	10	315.0	24	120.4	0.02350	1.19E-13	−12.92
C-2358	730	10	240.0	24	133.8	0.01890	1.26E-13	−12.90
C-2570	680	10	935.0	24	178.2	0.00883	1.51E-14	−13.82
C-2576	660	10	769.0	24	198.0	0.00280	5.83E-15	−14.23
C-2623	600	10	1200.0	24	211.9	0.00053	7.03E-16	−15.15
C-2624	730	20	240.0	24	172.9	0.00107	7.13E-15	−14.15
C-2675	730	10	240.0	24	6.7	—	—	—
C-2688	680	10	240.0	56	261.5	0.00070	2.53E-14	−13.60
C-2701	680	20	240.0	24	272.5	0.00016	1.05E-15	−14.98
C-2713	630	10	1200.0	24	201.0	0.00111	1.48E-15	−14.83
C-2764	680	10	240.0	56	282.3	0.00038	1.36E-14	−13.86
C-2777	680	10	240.0	24	174.3	0.00066	4.42E-15	−14.35
C-2785	730	10	240.0	87	270.2	0.00027	2.35E-14	−13.63
C-2796	730	10	240.0	56	262.2	0.00078	2.85E-14	−13.55
C-2799	730	10	0.178	24	254.1	0.00134	1.21E-11	−10.92
C-2800	730	10	24.0	24	197.6	0.00057	3.81E-14	−13.42
C-2801	730	10	48.0	24	190.3	0.00111	3.70E-14	−13.43
C-2802	680	10	240.0	87	258.4	0.00020	1.78E-14	−13.75
C-3049	630	10	480.0	24	211.1	0.00027	9.00E-16	−15.05
C-3051	680	20	336.0	24	196.8	0.00063	3.00E-15	−14.53

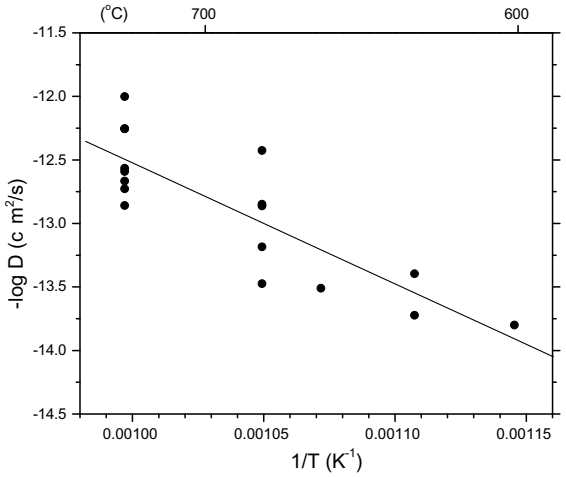

Fig. 5. Arrhenius plot of diffusion coefficients vs. reciprocal absolute temperature calculated for the 10 kbar experimental bulk loss data using an spherical diffusion model.

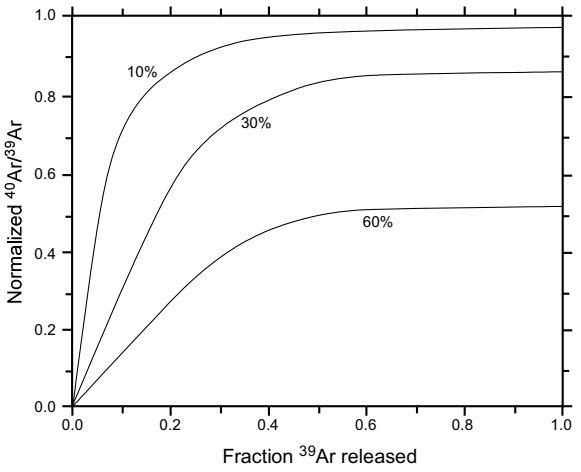

Fig. 6. Theoretical $^{40}Ar/^{39}Ar$ age spectra for a plane sheet geometry outgassed from a single diffusion domain (McDougall and Harrison, 1999). The convex form of age spectra from a single domain contrast with the sigmoidal form of the hydrothermally treated samples which are characteristic of multiple diffusion domains.

Robbins (1972) obtained, the distinctively sigmoidal form of the treated sample age spectra (Fig. 2) differs substantially from that expected of a sample containing a single diffusion length scale. Despite >50% apparent fractional loss in several of the hydrothermal runs, calculated ages in the final steps of gas release are close to the 326 Ma age of the starting material (Fig. 2). This is clearly inconsistent with diffusive loss from a single domain size, which is characterized by convex age spectra (Fig. 6). SEM textural characterization of the run products show that, despite careful pre-experiment sizing, the grain size population is non-uniform. As a proportion of the total volume, the nominal size grains dominate but many small grains are also present in both the pre- and the post-treatment muscovite samples (Célérier, 2007). SEM imaging also revealed that treated grains are somewhat kinked and creased suggesting that some crystal deformation was experienced, perhaps upon application of pressure while the sample was at room temperature. If so, $^{40}Ar^*$ may have been lost from the crystals by mechanical processes reducing the diffusion domain size of some grains.

The observation of grain size variability and the distinctive form of the age spectra indicate that $^{40}Ar^*$ loss is occurring from more than one diffusion domain size. The existence of two or more domains, widely separated in size, would explain why young ages are observed well into the

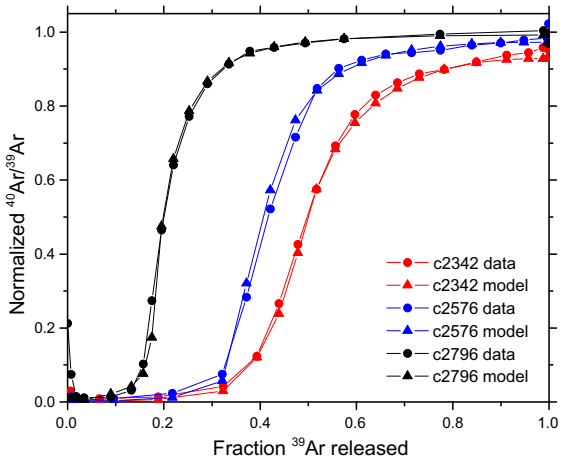

Fig. 7. Measured and model age spectra for samples (C-2342, C-2576, C-2796) representing the range of $^{40}Ar^{*}$ degassing behavior seen in this study.

gas release while ages as old as ca. 330 Ma are still seen in the last steps (Fig. 7). Most importantly, the presence of more than one diffusion domain has significant implications for the derivation of Arrhenius parameters for muscovite from the degassing data. In the next section we introduce a model to test this hypothesis and deconvolve the contributions of the various diffusion domain sizes to the $^{40}Ar^{*}$ total loss. Once we have accurately determined values of D for the largest intact domain (i.e., the nominally measured size), we can return to the determination of an Arrhenius law for Ar in muscovite.

5. MULTI-DIFFUSION DOMAIN SIZE MODEL

A model was constructed to simulate the effects of multiple diffusion domain sizes on the form of $^{40}Ar/^{39}Ar$ age spectra. For a sample outgassed over duration Δt_1, the $^{40}Ar^{*}/^{39}Ar$ ratio observed in the laboratory for any fractional loss of ^{39}Ar due to *in vacuo* heating of duration $\Delta t'$ is:

$$\frac{^{40}Ar^{*}}{^{40}Ar_K} = \frac{C_0}{C_{39}} \frac{(\sum_{n=1}^{\infty} \exp[-n^2\pi^2 D(\Delta t_1 + \Delta t')/r^2])}{[\sum_{n=1}^{\infty} \exp(-n^2\pi^2 D\Delta t'/r^2]} \quad (2)$$

where r is the diffusion domain size and C_0 is the concentration of $^{40}Ar^{*}$ produced prior to the outgassing event, Δt_1. The loss parameter is represented by the dimensionless Fourier number ($Fo = Dt/r^2$). Individual $^{40}Ar/^{39}Ar$ spectra for each domain size are then summed according to their volumetric proportions yielding the total gas release at each step in the model heating experiment. An $^{40}Ar/^{39}Ar$ spectrum can then be constructed by simultaneously solving the fractional loss (f) equation for spherical geometry (Crank, 1975) at each model heating step:

$$f = 1 - \frac{6}{\pi^2} \sum_{n=1}^{\infty} \frac{1}{n^2} \exp(-Dn^2\pi^2\Delta t'/r^2) \quad (3)$$

For efficiency of calculation, a spherical geometry was used rather than the infinite cylinder which requires use of the computationally expensive Bessel function. This may seem non-intuitive given the obvious anisotropy of micas, but the fractional loss curves for sphere and cylinder are similar in form in the range $0 < f < 0.5$ (McDougall and Harrison, 1999) and result in differences in calculated D of only a factor of two. Thus any introduced errors are insignificant provided the same diffusion geometry that is used to estimate Arrhenius parameters is also applied to calculation of T_c (Lovera et al., 1991).

To prepare for the modeling, data from each age spectrum were first normalized to the 326 Ma age of the untreated sample (or the oldest age in the spectrum for those cases with higher apparent ages). These input files were then used to calculate synthetic $^{40}Ar/^{39}Ar$ spectra by summing solutions for Eqs. (2) and (3) over n diffusion domains. Each model run requires three input parameters per domain, Fo, R, and V, where Fo_i is the Fourier number of the i-th domain, R_i is the retentivity of the i-th domain relative to the largest domain, and V_i is the volumetric proportion of the i-th domain (such that $\Sigma V_i\,(1,\ldots,n) = 1$). While there appear to be six input parameters for the two domain case, there are in fact only three since $Fo_2 = Fo_1.R_2$, $R_1 = 1$, and $V_2 = 1 - V_1$, where subscript 1 refers to the largest domain. Similar logic applies to the case of three or more domains. The best fit model is obtained by minimizing a misfit function between the actual age spectrum and randomly generated models.

In Fig. 7 we show three examples of model fits (C-2342, C-2576, C-2796) to normalized age spectra with varying degrees of $^{40}Ar^{*}$ loss. We emphasize that all runs yield fits of similar quality. The sensitivity of the model misfit function was assessed for the two domain case by varying each of these parameters independently (while keeping the other two constant), within a range bracketing their approximate

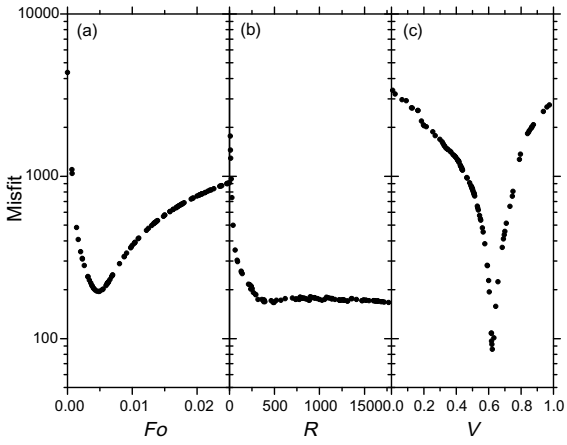

Fig. 8. Exploration of model parameter sensitivity to the fit between synthetic and *in vacuo* generated age spectra for C-2624 over specified parameter ranges for two domains. In (a), (b), (c) each dot represents a model run. (a) Sensitivity of misfit function to changes in the hydrothermal Fourier number (Fo) of the large domain. (b) Sensitivity of the misfit function to changes in the relative decrease in retentivity of the small relative to the large domain (R). (c) Sensitivity of the misfit function to changes in the relative volume (V) of the small domain as a proportion of 1.

best fit values for sample C-2342. Results of these calculations (Fig. 8) show that the model is sensitive to all parameters, but most strongly to the volumetric proportions of the large and small domains; 20% variance results in model fit changes of up to three orders of magnitude (Fig. 8c). This is because in the numerical simulations, V is important in establishing the position of the steep portion of in vacuo gas release. The degree of fit between model and C-2342 from adjustments to Fo varies by four orders of magnitude between 0 and 0.005 but is less sensitive above this value (Fig. 8a). Variations in Fo result in shifts in the maximum age retained by the sample in the final steps of gas release, but also affect the overall form of the age spectrum. Smaller Fo results in ages of ca. 326 Ma in the final steps, higher Fo values result in the final steps of gas release yielding ages $<$326 Ma (Fig. 7). Finally, the degree of fit between model and C-2342 is strongly sensitive to variations in the retentivity of the small domains (R) in the range 0 to $\sim$200 (Fig. 8b). Further decreases in retentivity do not greatly affect the fit between the model and C-2342, although in the case of some other samples the quality of fit decreases significantly with increasing R greater than the optimal minimum value.

The best fit model parameters were obtained by minimizing the misfit function for 10,000 random models, run using a range of Fo, R, and V values selected to avoid conflict with the boundary conditions. We first experimented with a two domain model and found that results matched the first order form of the observed age spectra reasonably well. However, consistent misfits to the sigmoidal portion of the degassing patterns were seen. This was unsurprising as SEM images (Fig. 3) show that the particle size distribution is not clearly bi-modal. Failure to accurately fit the transitional region could result in inaccurate values of Fo calculated for the largest domain, leading to an inaccurate estimation of the Arrhenius parameters. A three domain model yielded significantly improved results for most samples, whereas experiments adding a fourth or fifth domain were of negligible benefit and hence considered unnecessary.

The excellent fits between the numerical and experimental data (Fig. 7) is evidence that vacuum degassing of hydrothermally treated muscovite is well-described by a diffusion model containing multiple diffusion length scales. Having explored model parameter space to obtain the best match between the synthetic and measured spectra, we then systematically obtained fractional loss estimates from the treated samples by isolating the ^{40}Ar* lost from the grains that remained intact during the hydrothermal runs.

6. *IN VACUO* ARRHENIUS RESULTS

Perhaps even more surprising than the close correspondence of the muscovite ^{40}Ar/^{39}Ar age spectra to a simple diffusion model is that the rate of degassing *in vacuo* yields almost identical results to that of our hydrothermal experiments. For example, diffusion coefficients calculated from ^{39}Ar loss in step heating experiments on runs C-3049 and C-3051 not only yield the characteristic sigmoidal age spectrum form (Fig. 9a), but yield log (r/r_o) results (D/r^2 scaled

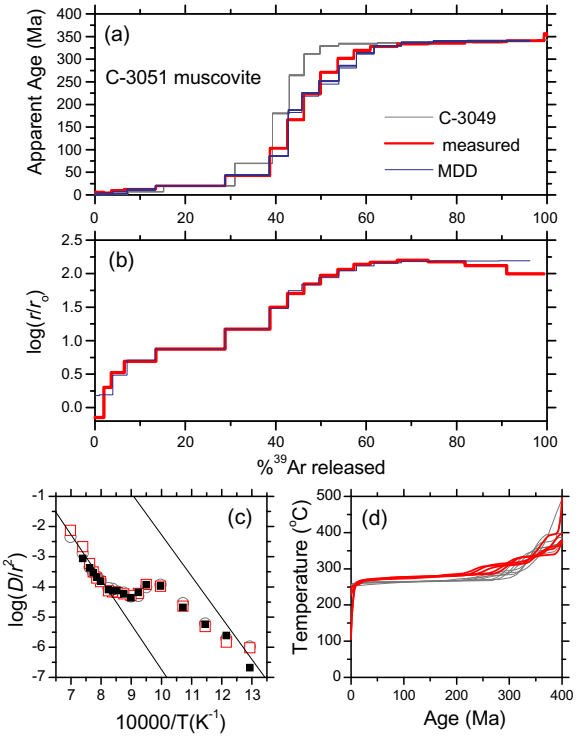

Fig. 9. (a) Age spectrum for muscovite C-3051 (red) together with MDD model (blue). Age spectrum for muscovite C-3049 is shown in grey. (b) Measured (red) and MDD model (blue) log (r/r_o) spectra for muscovite C-3051 calculated assuming $E = 63$ kcal/mol. (c) Arrhenius plot for muscovite C-3051 (red squares) together with MDD model (black squares). Arrhenius plot for muscovite C-3049 is shown as grey circles. (d) Thermal histories for muscovites C-3051 and C-3049 calculated using the MDD model assuming monotonic cooling.

to the initial gas release) that are high reminiscent of K-feldspars bearing multiple diffusion domains (Lovera et al., 1991). It is this capacity of K-feldspars to reveal correlations between age spectra (produced over millions of years) and laboratory Arrhenius data (produced in hours to days) that permits unique thermal history interpretations to be made (Harrison et al., 2005).

To characterize the behavior of muscovite during the step heating experiments, we heated aliquots of the 24 μm grain size in a 1 atm furnace programmed to reproduce the heating schedule used for the ANU ^{40}Ar/^{39}Ar analyses. Four runs, starting at 500 °C, were quenched after reaching each of 700, 840, 960, and 1020 °C. Optical and XRD analysis of the run products showed no evidence of either corundum or K-feldspar, the expected breakdown products of muscovite (Evans, 1965). Instead the observations are consistent with dehydroxylation of muscovite to a metastable form.

7. CALCULATION OF *D*

The targeted parameter of the modeling is the Fourier number (Fo) of the large domain induced during hydrothermal treatment. For run C-2342, the best fit between synthetic and real degassing behavior was achieved with an

Fo for the large grains of about 0.005 which is about a factor of five lower than that calculated from bulk-loss. This is entirely expected as the *Fo* derived from bulk-loss assumes a single diffusion domain.

For both the two and the three domain scenarios, best fits between model and real data were achieved with a higher proportion of large domains to small. This is consistent with the SEM images (Fig. 3; also see Célérier, 2007) which show that, as a proportion of the total volume, the large grains dominate. However, the best fit model estimate that ~30% of the diffusion domain volume is comprised of smaller domains is inconsistent with the observation that small grains account for <10% of the volume of C-2342. SEM images of C-2342 (Célérier, 2007) indicate that the sample is broadly characterized by grain size peaks at ~5, ~15, and ~45 μm suggesting that the smallest grains will be a factor of ~80 less retentive than the largest grains. In order to fit the degassing behavior of C-2342, the small diffusion domains in the model must be an order of magnitude less retentive than the large. The likely explanation for this apparent inconsistency is that the imaged grain size is not the same as diffusion domain size (i.e., sub-grain features also contribute to diffusion loss).

Examination of the experimental run products shows that recrystallization and new grain growth are negligible in the treated muscovites (Célérier, 2007; Fig. 3) and thus this is unlikely to explain the very low domain retentivities required by the best fit models for C-2342. However, we note that SEM imagery of the hydrothermally treated run products show that, relative to the untreated sample, the treated grains are kinked, creased and crystal surfaces are not as well defined. We attribute these textures to mechanical deformation that occurred during the high pressure runs. The standard practice of initiating the experiments "cold" such that the confining pressure is effectively attained while the sample is still at room temperature might produce a sub-grain network that could enhance $^{40}Ar^{*}$ loss. To test this hypothesis, we undertook a very short term experiment (C-2799); 10 min at 730 °C. The age spectrum for C-2799 shows much greater bulk $^{40}Ar^{*}$ loss (~20%) than would be predicted from diffusion alone (<1%). Relative to other runs at 730 °C, with durations between 24 and 315 h, C-2799 yields a *D* for the large domain that is orders of magnitude higher (Table 2). This result appears to affirm that changes to the diffusion domain structure occurring at very small (<1 μm) length scales are induced almost immediately upon pressurization, perhaps defined by cracks and planar dislocation features. However, after one day at 730 °C, these domains are essentially degassed and thus appear not to influence calculation of *D* for the longer runs.

Best fit solutions for the *Fo* parameter (Dt/r^2) for multi-diffusion domain models are given in Table 2 together with derived values of *D*. Several tests can be applied to gain insight into the mechanism of $^{40}Ar^{*}$ transport. First, linearity on an Arrhenius diagram is evidence that $^{40}Ar^{*}$ transport occurred primarily by a temperature-dependent mechanism. Results for the 10 kbar experiments longer than 10 min define a linear trend (Fig. 10), although scatter about the best fit line at 730 °C is seen, perhaps reflecting new muscovite grain growth and the greater Al:Si exchange experienced at the highest temperatures. Second, a plot of *f*

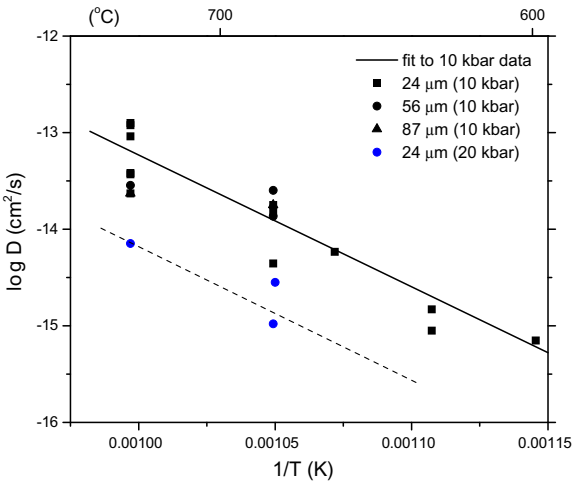

Fig. 10. Arrhenius plot of diffusion coefficients calculated from experimental data using a spherical diffusion model, against reciprocal absolute temperature.

vs. the square root of run duration, *t*, should correspond to diffusion theory. Fig. 11 shows calculated *f* for the six experiments at 730 °C using the 24 μm size fraction vs. $\sqrt{t}$. Also shown is the predicted curve of *f* vs. time for $D/a^2 = 9.0 \times 10^{-14}$ cm²/s (assuming a spherical geometry). With the exception of the 10 min run (C-2799), the experimental data plot reasonably close to the predicted curve, consistent with diffusion being the principal $^{40}Ar^{*}$ transport mechanism. Linear regression of the 10 kbar data (excluding C-2779 and C-2802) yields an *E* of 63 ± 7 kcal/mol and D_o of $2.3\ ^{+70}_{-2.2}$ cm²/s (Fig. 10). These values are substantially different from that calculated from the bulk-loss data (Fig. 5).

To investigate the role of pressure on Ar diffusion in muscovite, experiments at 20 kbar were undertaken at 730 and 680 °C. Calculated *D*'s from the 20 kbar data (Fig. 9) plot below the equivalent results at 10 kbar indicating a pressure effect on the diffusion of ^{40}Ar in muscovite. To ac-

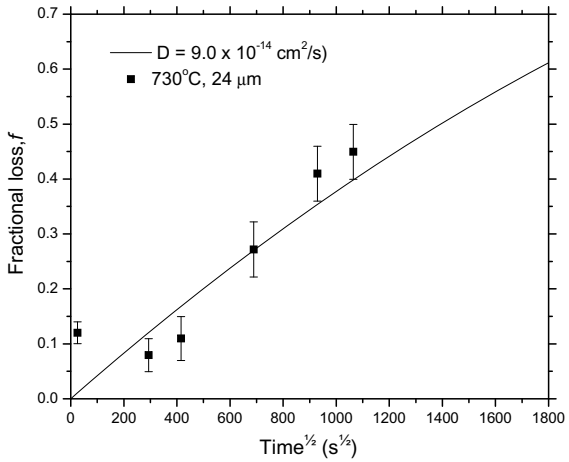

Fig. 11. Plot of the fractional ^{40}Ar loss (*f*) from hydrothermally treated muscovites vs. the square root of run duration. Data shown as squares are the 24 μm size fraction run at 730 °C and 10 kbar.

count for the extra work diffusing atoms must perform against confining pressure, a modified Arrhenius equation can be written as:

$$D = D_o \exp[-(E + PV^*)/RT] \quad (4)$$

where V^* is the activation volume of the diffusing species. Assuming the same activation energy, V^* can be directly calculated from the difference between the 20 and 10 kbar runs. Diffusion coefficients are reduced from their equivalent 10 kbar values by close to an order of magnitude which corresponds to an activation volume of $\sim 14\ cm^3/mol$. Although the relatively few higher pressure data preclude a precise estimate of V^*, this value is similar to that determined for biotite (Harrison et al., 1985).

8. DISCUSSION

8.1. Muscovite behavior during vacuum heating

A fundamental assumption of the age spectrum approach is that *in vacuo* $^{40}Ar^*$ loss occurs with the same geometry and over the same length scales as in Nature, although not necessarily by the same mechanism. The first application of the $^{40}Ar/^{39}Ar$ method was to meteorite samples which, containing anhydrous minerals (Turner et al., 1966), remained stable during vacuum heating and degassed Ar diffusively (Albarède, 1978). However, the age spectrum method proved generally unsuitable for some hydrous terrestrial minerals which are highly unstable *in vacuo* (McDougall and Harrison, 1999).

Our observation of diffusive degassing of Ar from hydrothermally treated muscovites *in vacuo* (Figs. 2 and 7; Electronic annexes EA-1 and EA-2) is consistent with numerous observations that $^{40}Ar/^{39}Ar$ age spectra of white micas can yield apparent diffusion loss profiles when partially overprinted (Hanson et al., 1975; Wijbrans and McDougall, 1986; Baldwin and Harrison, 1992; Grove, 1993). This contrasts with hydrous phases such as biotite which yield flat, convex upward, or irregular release patterns from samples that have experienced $^{40}Ar^*$ loss (Berger, 1975; Dallmeyer, 1975; Harrison et al., 1985; Gaber et al., 1988). Although hornblende has been found to degas Ar in a fashion that mimics diffusion (Harrison and McDougall, 1980; Harrison, 1981; Copeland et al., 1991), this reflects its decomposition by an inwardly propagating reaction front during vacuum heating (Lee et al., 1991; Wartho, 1995).

In contrast to biotite and hornblende, dioctahedral micas such as muscovite dehydroxylate to a metastable form that preserves the integrity of the 2:1 layer structure and the interlayer region (Guggenheim et al., 1987). A recent study of the dehydration behavior of muscovite up to 875 °C using *in situ* infrared microspectroscopy showed that muscovite progressively dehydrates with increasing temperature without breaking down (Tokiwai and Nakashima, 2007). Our 1 atm heating experiments show that dehydroxylated muscovite remains metastable up to at least 1020 °C. Grove (1993) performed $^{40}Ar/^{39}Ar$ step heating experiments on vacuum dehydroxylated white micas which revealed staircase age spectrum patterns characteristic of diffusive $^{40}Ar^*$ loss. Significantly, he found that Arrhenius parameters calculated from both untreated and dehydroxylated samples were essentially identical. This implies that either untreated natural micas transformed to their dehydroxylated form as they degassed during step heating or that the kinetics of ^{40}Ar loss of the hydroxylate and dehydroxylate are similar. In either case, it appears that ^{40}Ar gradients in white micas are preserved in, and can be revealed from, the metastable dehydroxylate phase. Sletten and Onstott's (1998) conclusion that age gradients in muscovite spectra reflect $^{40}Ar^*$ release from polyphase mixtures appears inconsistent with all of the aforementioned observations.

While it appears that muscovite can retain sufficient crystalline integrity to preserve and reveal $^{40}Ar/^{39}Ar$ gradients, it has been widely believed that the rate of Ar loss during vacuum heating is much faster than under hydrothermal conditions (Giletti, 1974; Grove, 1993; Sletten and Onstott, 1998). Surprisingly then, ^{39}Ar diffusion coefficients from our run products yield 'S' shaped Arrhenius plots (Fig. 9c) characteristic of K-feldspars (Lovera et al., 2002). In context of the multi-diffusion domain (MDD) model, the initially shallow slope is interpreted as the degassing of a relatively small, low-volume-fraction domain. This is followed by a steeper portion corresponding to the intrinsic E of the largest domain size. Surely not coincidentally, the slope of this portion of the curve yields an activation energy of ~65 kcal/mol – virtually identical to that obtained from the hydrothermal data (Fig. 10). The apparent D_o/r^2 of this array together with the sample grain size (24 μm radius used for runs C-3051) translates to a frequency factor of $\sim 40\ cm^2/s$ – marginally higher than the value obtained from the hydrothermal data of $\sim 2\ cm^2/s$ (Fig. 10). Even so, the comparison is inexact as it relates 10 kbar data with results obtained at effectively 0 kbar. Scaling D using 0.1 log unit/kbar (Fig. 10) indicates that the vacuum-derived D_o should be decreased by an order of magnitude leading to a comparison value of $\sim 4\ cm^2/s$. This remarkable similarity is reproducible. For example, the log (r/r_o) and Arrhenius data for C-3049, superimposed, respectively, in Fig. 9b and c, plot atop the results for C-3051 (as they should inasmuch as the same size fraction and essentially identical lab heating schedules were used in the two runs).

Modeling the log (r/r_o) spectrum gives an independent estimate of the volume fraction of the biggest domain (V_1) that is virtually identical to what we obtained from modeling the age spectrum alone. Because this parameter is essentially uniquely determined from the age spectrum (see Fig. 8c), there appears to be little gained from a joint inversion of the age and log (r/r_o) spectra to obtain V_1. We did, however, take the analogy with K-feldspar MDD one step further and inverted the age and log (r/r_o) spectra for C-3051 (assuming monotonic cooling and $E = 64$ kcal/mol) to obtain the thermal history shown in red in Fig. 9d. Although the slow cooling scenario is obviously unrealistic for our case where ^{40}Ar loss is caused by laboratory heating, the domain structure also sufficiently mimics a protracted (ca. 300 Ma) isothermal history at ~270 °C to converge to a single solution. This result is robust for the amount of $^{40}Ar^*$ loss as a virtually identical history is obtained for C-3049 (shown in grey in Fig. 9d). This is strong

evidence that muscovite can retain the Ar diffusion boundaries and mechanisms that define their natural retentivity during vacuum step heating. This may have profound implications for $^{40}Ar/^{39}Ar$ thermochronology.

If muscovites can be routinely utilized for MDD modeling, the large expanses of low grade metamorphic terranes previously not accessible by high resolution, continuous thermochronometry (Harrison et al., 2005) could see tremendous improvement in the quality of thermal history reconstructions. However, hydrothermal treatment may have altered the run products in ways that enhanced their stability *in vacuo* relative to natural samples. We tested this hypothesis by analyzing the starting material and some run products by Fourier Transform Infrared Spectroscopy. We observed that the starting material and run products (C-2342 and C-2570) display the same dominant hydrous peak at 3625 cm^{-1} indicating that muscovite remained stable, and OH-bonding remained unchanged, during hydrothermal treatment.

There is relatively little documentation in the literature that relates muscovite $^{40}Ar/^{39}Ar$ age spectra produced during vacuum step heating to their associated Arrhenius plots. Lovera et al. (2002) provided one such example in which a sinuous, stair-case type muscovite age spectrum is positively, albeit not strongly, correlated with its log (r/r_o) plot ($r^2 = 0.76$). Our experience suggests that fine grained micas, such as those used in this study, are less likely to experience catastrophic degassing during vacuum heating than much larger flakes, possibly reflecting a size threshold above which recovery of diffusion information is not possible. In any case, it is clear that further attention to this issue could yield substantial benefits.

8.2. Comparison with previous results

We believe that the contrast in activation energy for Ar diffusion in muscovite between this study and that of Robbins (1972) largely reflects limitations in the methods he used. Comparing absolute ^{40}Ar concentrations measured by isotope dilution before and after heating is insensitive to small (<5%) $^{40}Ar^*$ losses. The average f in the Robbins (1972) study was only 7% and the lower temperature (i.e., lower f) data are thus particularly unreliable. Indeed, half of all runs in that study were annotated as problematic in terms of capsule leakage during hydrothermal heating or quantitative measurement of $^{40}Ar^*$ loss. However, the experiments he undertook at the highest temperature (700 °C), which all yielded >10% $^{40}Ar^*$ loss, plot within half a log unit of our Arrhenius relationship when corrected for the different pressures used (i.e., 0.1 log unit/kbar; Fig. 10). Thus the more reliable results of the Robbins (1972) study appear broadly consistent with our data.

A limitation on applying laboratory measurements of diffusion to geochronological problems is that results must typically be extrapolated many orders of magnitude down temperature to the realm of isotopic closure. This can be mitigated by use of analysis methods capable of measuring diffusion profiles at the nm-scale (e.g., Cherniak et al., 2004) but, as noted earlier, no such approaches are available for measurement of Ar diffusion in minerals commonly used for $^{40}Ar/^{39}Ar$ dating. Although geologically 'anchoring' experimentally-derived diffusion laws by relating disturbance of an isotopic system in response to natural thermal excursions is appealing, uncertainties in constraining the thermal budget often preclude accurate estimates (e.g., Hart, 1964).

Kirschner et al. (1996) estimated log $D_{320\,°C} = -22.1$ (cm^2/s) for Ar in muscovite from $^{40}Ar/^{39}Ar$ age gradients in white micas grown at a peak temperature of 320 °C during nappe development. This study was unusually well-constrained in that peak temperature was not estimated from a thermal model but rather determined directly from oxygen isotope thermometry. To compare their estimated D, which is substantially lower than that predicted by Robbins (1972), with our data we must adjust their datum to relate to the pressure under which our experiments were undertaken. Given that Ar diffusion in muscovite decreases by about 0.1 log unit/kbar (Fig. 10), we have reduced their ca. 3 kbar estimate to −22.8 (cm^2/s) to directly compare to our 10 kbar results. When so corrected, the Kirschner et al. (1996) datum plots directly on the extrapolation of our 10 kbar data array (Fig. 12). Linear regression of the combined dataset yields an apparent E of 63.5 ± 1.8 kcal/mol and associated D_o of $4^{+6.8}_{-2.5}$ cm^2/s. This close agreement builds confidence in the efficacy of both methods.

8.3. Ionic porosity model

Fortier and Giletti (1989) advocated an empirical approach to predicting diffusivities based on the systematic variation of measured oxygen diffusion in minerals relative to their ionic porosity (Z). Results for micas, however, were discordant to the overall trend. This was attributed to the fact that ionic porosities for the interlayer regions of micas, the likely path for Ar transport, are much larger than for the bulk mineral. 'Effective' ionic porosities for micas were estimated by projecting measured oxygen diffusion coeffi-

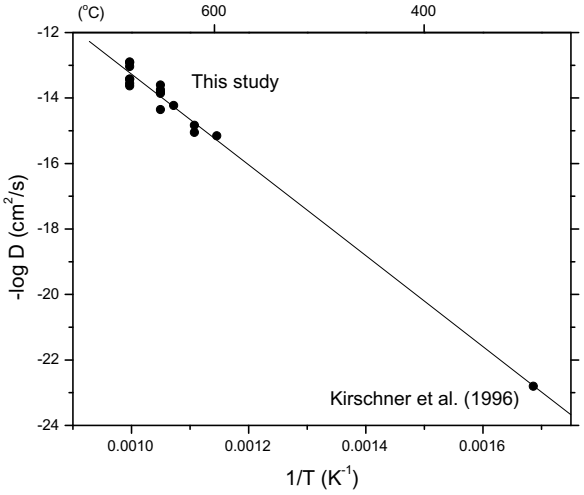

Fig. 12. Arrhenius plot of diffusion coefficients calculated from hydrothermally treated muscovites together with natural estimate of D from Kirschner et al. (1996).

cients onto the relationship defined by log D vs. bulk Z in non-phyllosilicates. Values of Z calculated in this way led to model coefficients for Ar that appeared to fit the relatively scant data then available. However, experimental diffusion data for muscovite were too poorly constrained to determine effective ionic porosity for that phase.

We have revisited this model with our new result and note that, with the exception of biotite (Harrison et al., 1985; Grove and Harrison, 1996), laboratory Ar diffusion data (i.e., hornblende, Harrison, 1981; muscovite, this study; phlogopite, Giletti, 1974; K-feldspar, Foland, 1974) yield well-correlated relationships between log D and Z (hornblende Z from Dahl, 1996; all others from Fortier and Giletti, 1989) as a function of temperature. For example, at 500 °C, the array is of the form log D (cm^2/s) $= -40 + 0.6 \cdot Z$ ($r^2 = 0.98$). This correlation suggests a much higher degree of coherence among the various silicate groups than previously inferred (albeit with biotite not fitting this apparent trend) and may be evidence of a more systematic relationship between diffusivity and Z. Without many more experimental data, however, there is little to be gained by pursuing this approach at the present.

8.4. Closure temperature

Our preferred Arrhenius parameters ($E = 64$ kcal/mol, $D_o = 4$ cm^2/s) correspond to a muscovite closure temperature (T_c; Dodson, 1973) of 425 °C for an effective diffusion radius of 100 μm and 10 °C/Ma cooling rate. Note that for these parameters, the bulk-loss array (Fig. 5) predicts a T_c of ~310 °C – over 100 °C lower.

We note that our experiments were undertaken at substantially higher pressure than typical for Ar closure in white mica. With the exception of phengitic micas under blueschist facies conditions, temperatures of ca. 450 °C are generally reached in the crust at ~5 kbar. Determination of V^* permits modification of the Arrhenius law for application to lower pressures. Our estimated V^* of 14 cm^3/mol corresponds to an increase of D_o at 5 kbar of a factor of five relative to that at 10 kbar (i.e., $D_o = 20$ cm^2/s). For the same parameters as the calculation in the preceding paragraph, this predicts a closure temperature of 405 °C (i.e., 20 °C lower).

Fig. 13 shows the variation of T_c with cooling rate and diffusion dimension for the equivalent 5 kbar Arrhenius parameters. For most cases, predicted closure temperatures are substantially higher than that advocated as a nominal value (e.g., 350 °C; Hodges, 1991). For example, a T_c of 430 °C arises for a 100 μm diffusion radius cooling at 100 °C/Ma or a 500 μm diffusion radius cooling at 2 °C/Ma – both possible conditions for white micas in convergent margin environments. It has previously been speculated that V^* for white mica is sufficiently large that phengitic micas could be characterized by a T_c as high as 550 °C under blueschist conditions (e.g., Lister and Baldwin, 1996). Although the estimated V^* is not anomalously high, the overall higher retentivity of Ar in white micas seen in this study supports their broader conclusion regarding closure temperature of phengite at high pressure.

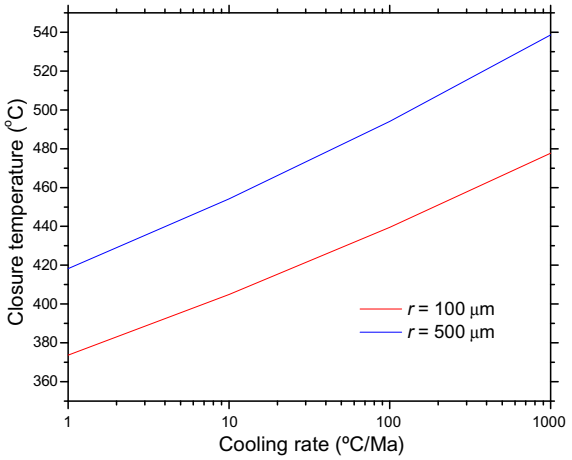

Fig. 13. Variation of T_c with cooling rate and diffusion dimension for Arrhenius parameters appropriate to 5 kbar pressure ($E = 64$ kcal/mol and $D_o = 20$ cm^2/s).

We remind potential users that our diffusion law for Ar in muscovite was calculated assuming radial diffusion in a sphere and thus thermochronological data from real samples must be handled, and errors propagated, using equations and models based on spherical geometry.

9. CONCLUSIONS

^{40}Ar/^{39}Ar analyses of muscovite sample MUS-1 treated at high temperature and water pressure in a piston-cylinder apparatus yield a linear array indicative of ^{40}Ar* transport by volume diffusion. However, the *in vacuo* ^{40}Ar/^{39}Ar degassing behavior of the hydrothermally treated material is characterized by both convex and concave forms. This distinctive form of the age and Arrhenius spectra differs from that expected from a sample that has been outgassed from a single diffusion domain. SEM textural characterization of the run products shows that, despite careful pre- and post-hydrothermal experiment sieving of the muscovites, the size population of the run material is not uniform. We investigated the hypothesis that the form of *in vacuo* gas release is due to loss of ^{40}Ar* from multiple diffusion domains. A numerical model constructed to test this hypothesis yields excellent fits between synthetic and actual degassing spectra (both age and log (r/r_o)), supporting the multiple diffusion domain hypothesis. However, the presence of multiple diffusion domains in the hydrothermal run products impact calculated diffusion parameters. Deconvolution of the contribution of multiple diffusion domains to the experimentally determined factional loss yield estimates of D that are substantially lower than that assuming bulk-loss from a single domain size. Diffusion data generated in this manner indicate an activation energy of E of 63 ± 7 kcal/mol and log D_o of $2.3^{+70}_{-2.2}$ cm^2/s and an activation volume of ~14 cm^3/mol. These values correspond to a closure temperature (T_c) of 425 °C for a muscovite grain with a 100 μm radius cooling at 10 °C/Ma at 10 kbar and ca. 405 °C at 5 kbar. We found that the age and log (r/r_o) spectra for the hydrothermally treated muscovite samples show a remarkable degree of correlation indicating that

muscovite can retain the Ar diffusion boundaries and mechanisms that define their natural retentivity during vacuum step heating. This observation has tremendous potential implications for diversifying high resolution $^{40}Ar/^{39}Ar$ thermochronology.

ACKNOWLEDGMENTS

We thank the Australian Research Council and National Science Foundation for grant support, Jim Dunlap for use of the ANU $^{40}Ar/^{39}Ar$ facility, Dean Scott for technical assistance, Peter Zeitler, Suzanne Baldwin, and Rick Ryerson for helpful reviews, and Oscar Lovera for assistance with the modeling.

APPENDIX A. SUPPLEMENTARY DATA

Supplementary data associated with this article can be found, in the online version, at doi:10.1016/j.gca.2008.09.038.

REFERENCES

Albarède F. (1978) Recovery of spatial isotope distributions from stepwise degassing data. *Earth Planet. Sci. Lett.* **39**, 387–397.

Baldwin S. L., Harrison T. M. and Fitz Gerald J. D. (1990) Diffusion of ^{40}Ar in metamorphic hornblende. *Contrib. Mineral. Petrol.* **105**, 691–703.

Baldwin S. L. and Harrison T. M. (1992) The P–T–t history of blocks in serpentinite-matrix melange, west-central Baja California. *Geol. Soc. Am. Bull.* **104**, 18–31.

Berger G. W. (1975) $^{40}Ar/^{39}Ar$ step heating of thermally overprinted biotite, hornblende and potassium feldspar from Eldora, Colorado. *Earth Planet. Sci. Lett.* **26**, 387–408.

Célérier J. (2007) The structural and thermal evolution of the Kumaun and Garwhal Lesser Himalaya, India. PhD Thesis. The Australian National University.

Chatterjee N. D. and Johannes W. (1974) Thermal stability and standard thermodynamic properties of synthetic 2M 1-Muscovite, $KAl_2[AlSi_3O_{10}(OH)_2]$. *Contrib. Mineral. Petrol.* **48**, 89–114.

Cherniak D. J., Watson E. B., Grove M. and Harrison T. M. (2004) Pb diffusion in monazite: a combined RBS/SIMS study. *Geochim. Cosmochim. Acta* **68**, 829–840.

Copeland P., Harrison T. M., Hodges K. V., Maruejol P., Lefort P. and Pêcher A. (1991) An Early Pliocene thermal disturbance of the Main Central Thrust, Central Nepal – implications for Himalayan tectonics. *J. Geophys. Res.* **96**, 8475–8500.

Crank J. (1975) *The Mathematics of Diffusion*, second ed. Clarendon Press, Oxford.

Dahl P. S. (1996) The effects of composition on retentivity of Ar and O in hornblende and related amphiboles: a field-tested empirical model. *Geochim. Cosmochim. Acta* **60**, 3687–3700.

Dallmeyer R. D. (1975) $^{40}Ar/^{39}Ar$ ages of biotite and hornblende from a progressively remetamorphosed basement terrane – their bearing on interpretation of release spectra. *Geochim. Cosmochim. Acta* **39**, 1655–1669.

Dodson M. H. (1973) Closure temperature in cooling geochronological and petrological systems. *Contrib. Mineral. Petrol.* **40**, 259–274.

Evans B. W. (1965) Application of reaction-rate method to the breakdown equilibria of muscovite plus quartz. *Am. J. Sci.* **263**, 647–667.

Foland K. A. (1974) Diffusion of ^{40}Ar in orthoclase. *Geochim. Cosmochim. Acta* **38**, 151–161.

Fortier S. M. and Giletti B. J. (1989) An empirical model for predicting diffusion coefficients in silicate minerals. *Science* **245**, 1481–1484.

Gaber L. J., Foland K. A. and Corbato C. E. (1988) On the significance of ar release from biotite and amphibole during $^{40}Ar/^{39}Ar$ vacuum heating. *Geochim. Cosmochim. Acta* **52**, 2457–2465.

Giletti B. (1974) Studies in diffusion 1: Ar in phlogopite mica. In *Geochemical Transport and Kinetics*, 634 (eds. A. Hofmann, B. J. Gilleti, H. S. Yoder and R. A. Yund). Carnegie Inst. of Wash. Publ., pp. 107–115.

Grove M. (1993) Thermal histories of Southern California basement terranes. Ph.D. Thesis. University of California, Los Angeles, p. 419.

Grove M. and Harrison T. M. (1996) $^{40}Ar^{*}$ diffusion in Fe-rich biotite. *Am. Min.* **81**, 940–951.

Guggenheim S., Chang Y.-H. and Koster van Gross A. F. (1987) Muscovite dehydroxylation: high temperature studies. *Am. Min.* **7**, 537–550.

Hames W. E. and Bowring S. A. (1994) An empirical evaluation of the Ar diffusion geometry in muscovite. *Earth Planet. Sci. Lett.* **124**, 161–167.

Hanson G. N., Simmons K. R. and Bence A. E. (1975) $^{40}Ar/^{39}Ar$ spectrum ages for biotite, hornblende and muscovite in a contact metamorphic zone. *Geochim. Cosmochim. Acta* **39**, 1269–1277.

Harrison T. M. (1981) Diffusion of ^{40}Ar in hornblende. *Contrib. Mineral. Petrol.* **78**, 324–331.

Harrison T.M., Grove M., Lovera O.M. and Zeitler, P.K. (2005) Continuous thermal histories from closure profiles. In *In Low Temperature Thermochronology: Techniques, Interpretations and Applications, Revs. Mineral. Geochem*. 58, 389–409.

Harrison T. M., Duncan I. and McDougall I. (1985) Diffusion of ^{40}Ar in biotite – temperature, pressure and compositional effects. *Geochim. Cosmochim. Acta* **49**, 2461–2468.

Harrison T. M. and McDougall I. (1980) Investigations of an intrusive contact, Northwest Nelson, New-Zealand. 2. Diffusion of radiogenic and excess ^{40}Ar in hornblende revealed by $^{40}Ar/^{39}Ar$ age spectrum analysis. *Geochim. Cosmochim. Acta* **44**, 2005–2020.

Hart S. R. (1964) The petrology and isotopic-mineral age relations of a contact zone in the Front Range, Colorado. *J. Geol.* **72**, 493–525.

Heizler M. T., Perry F. V., Crowe B. M., Peters L. and Appelt R. (1999) The age of lathrop wells volcanic center: an $^{40}Ar/^{39}Ar$ dating investigation. *J. Geophys. Res.* **104**, 767–804.

Hodges K. V. (1991) Pressure–temperature–time paths. *Ann. Rev. Earth Planet. Sci.* **19**, 207–236.

Kirschner D. L., Cosca M. A., Masson A. and Hunziker J. C. (1996) Staircase $^{40}Ar/^{39}Ar$ spectra of fine-grained white mica: Timing and duration of deformation and empirical constraints on argon diffusion. *Geology* **24**, 747–750.

Lee J. K. W., Onstott T. C., Cashman K. V., Cumbest R. J. and Johnson D. (1991) Incremental heating of hornblende in vacuo – implications for $^{40}Ar/^{39}Ar$ geochronology and the interpretation of thermal histories. *Geology* **19**, 872–876.

Lister G. S. and Baldwin S. L. (1996) Modelling the effect of arbitrary P–T–t histories on Ar diffusion in minerals using the MacArgon program for the Apple Macintosh. *Tectonophysics* **253**, 83–109.

Lovera O. M., Grove M. and Harrison T. M. (2002) Systematic analysis of K-feldspar $^{40}Ar/^{39}Ar$ step-heating experiments II: relevance of laboratory K-feldspar argon diffusion properties to Nature. *Geochim. Cosmochim. Acta* **66**, 1237–1255.

Lovera O. M., Richter F. M. and Harrison T. M. (1991) Diffusion domains determined by ^{39}Ar release during step heating. *J. Geophys. Res.* **96**, 2057–2069.

McDougall I. and Harrison T. M. (1999) *Geochronology and Thermochronology by the 40Ar/39Ar Method*, second ed. Oxford University Press.

Purdy J. W. and Jäger E. (1976) K–Ar ages on rock-forming minerals from the Central Alps. *Mem. Inst. Geol. Min. Univ. Padova*, 30.

Renne P. R., Swisher C. C., Deino A. L., Karner D. B., Owens T. L. and DePaolo D. J. (1998) Intercalibration of standards, absolute ages and uncertainties in $^{40}Ar/^{39}Ar$ dating. *Chem. Geol.* **145**, 117–152.

Robbins G.A. (1972) Radiogenic Ar diffusion in muscovite under hydrothermal conditions. M.S Thesis, Brown University, Providence, RI.

Ryerson F. J. (1987) Diffusion measurements: experimental methods. In *Methods of Experimental Geophysics* (eds. C. G. Sammis and T. Henyey), pp. 89–129. vol. 24. Academic Press.

Sletten V. W. and Onstott T. C. (1998) The effect of the instability of muscovite during in vacuo heating on $^{40}Ar/^{39}Ar$ step heating spectra. *Geochim. Cosmochim. Acta* **62**, 123–141.

Stieger R. H. and Jäger E. (1977) Subcommission on Geochronology – convention on use of decay constants in geochronology and cosmochronology. *Earth Planet. Sci. Lett.* **36**, 359–362.

Tetley N., McDougall I. and Heydegger H. R. (1980) Thermal-neutron interferences in the $^{40}Ar/^{39}Ar$ dating technique. *J. Geophys. Res.* **85**, 7201–7205.

Tokiwai K. and Nakashima S. (2007) Dehydration behaviour of muscovite by in situ infrared microspectroscopy. *Geochim. Cosmochim. Acta* **71**, A1026.

Turner G., Miller J. A. and Grasty R. L. (1966) The thermal history of the Bruderheim meteorite. *Earth Planet. Sci. Lett.* **1**, 155–157.

Wartho J. A. (1995) Photoemission electron-microscopy (PEEM) heating investigations of a natural amphibole sample. *Min. Mag.* **59**, 121–127.

Wijbrans J.R. (1985) Geochronology of metamorphic terrains by the $^{40}Ar/^{39}Ar$ age spectrum method. Ph.D. Thesis, Australian National University, Canberra.

Wijbrans J. R. and McDougall I. (1986) $^{40}Ar/^{39}Ar$ dating of white micas from an alpine high-pressure metamorphic belt on Naxos (Greece) – the resetting of the Ar isotopic system. *Contrib. Mineral. Petrol.* **9**, 187–194.

Associate editor: F.J. Ryerson